Electrodeposited gold nanoparticles on glassy carbon: Correlation between nanoparticles characteristics and oxygen reduction kinetics in neutral media

Guillaume Gotti [a,b,c,d], Katia Fajerwerg [c,d,*], David Evrard [a,b,**], Pierre Gros [a,b,1]

[a] Université de Toulouse, UPS, INPT, Laboratoire de Génie Chimique, 118 route de Narbonne, F-31062 Toulouse, France
[b] CNRS, Laboratoire de Génie Chimique, F-31062 Toulouse, France
[c] CNRS, LCC (Laboratoire de Chimie de Coordination), 205 route de Narbonne, F-31077 Toulouse, France
[d] Université de Toulouse, UPS, INPT, LCC, F-31077 Toulouse, France

Keywords:
Gold nanoparticles electrodeposition
Oxygen reduction reaction
Neutral media
Koutecky–Levich analysis
Electrochemical kinetics

A B S T R A C T

Gold nanoparticles (AuNPs) were deposited onto glassy carbon (GC) by constant potential electrolysis (CPE) using various sets of potential and duration from −0.3 to 0.7 V/SHE and 10 to 1800 s, respectively. The physico-chemical characteristics of the as-obtained deposits were investigated by cyclic voltammetry (CV) in H_2SO_4, field emission gun scanning electron microscopy (FEG-SEM), and Pb underpotential deposition (UPD). Their performances toward the oxygen reduction reaction (ORR) in a NaCl–$NaHCO_3$ (0.15 M/0.028 M, pH 7.4) neutral solution were examined and correlated to AuNPs size and density. The best results were obtained using the deposits which exhibited a high density ($555 \pm 49\ \mu m^{-2}$) of relatively small AuNPs (25 ± 12 nm). The Koutecky–Levich treatment was systematically applied to all the deposits in order to determine the number of electrons n exchanged for the ORR in the potential range from 0.1 to −1.0 V/SHE. The values of the cathodic transfer coefficients βn were also extracted and compared to the values reported for unmodified GC and bulk Au. A map of the βn values as a function of AuNPs electrodeposition potential and duration was also provided.

1. Introduction

The oxygen (O_2) reduction reaction (ORR) is probably one of the most studied redox processes in the literature, both from the mechanistic [1–3] and kinetic [4–8] points of view. Amongst the numerous works dealing with this electrochemical system, the Damjanovic model is of particular interest which describes the ORR as a multi-electron reaction [9]. Thus, O_2 reduction may be achieved by a four-electron "direct" pathway (Eq. (1)) or via two successive bielectronic steps involving hydrogen peroxide (H_2O_2) as an intermediate species (Eqs. (2) and (3)) [10–12]:

$$O_2 + 4H^+ + 4e^- \rightarrow 2H_2O \quad E^\circ = 1.23\,V/SHE \tag{1}$$

$$O_2 + 2H^+ + 2e^- \rightarrow H_2O_2 \quad E^\circ = 0.70\,V/SHE \tag{2}$$

$$H_2O_2 + 2H^+ + 2e^- \rightarrow H_2O \quad E^\circ = 1.78\,V/SHE \tag{3}$$

Gnanamuthu and Petrocelli have also analyzed a series of more complex reduction paths for O_2 reduction on noble metals (Pt, Pd, Au) and alloys (Pd–Au and Pt–Au) [13].

This standing interest in ORR is mainly due to the wide range of application domains it is involved in, from chemical or biochemical analysis [14,15] to industrial fields such as pharmaceutics [16], corrosion [17] or energy storage and conversion [18,19]. For instance, O_2 may be used directly as oxidation agent in food process [20]. It may be also reduced into H_2O_2 which can be further used as a sterilizing agent [16]. More recently the development of fuel cells drove a particular emphasis on ORR kinetic study in acidic or basic media on various catalysts including carbon-based materials, enzymes, macrocycles or coordination complexes of transition metals [21]. Amongst the numerous materials used, nanoparticles (NPs), and especially gold nanoparticles (AuNPs) have been extensively studied [22,23]. In acidic media, kinetic data have been obtained by electrochemical impedance spectroscopy [24], rotating ring disk electrode [25] and scanning electrochemical microscopy [26]. In many studies the AuNPs electrocatalytic activity toward ORR has been found to be size [25–27] and crystal structure-dependent

* Corresponding author at: CNRS, LCC (Laboratoire de Chimie de Coordination), 205 route de Narbonne, F-31077 Toulouse, France. Tel.: +33 5 61 33 31 30; fax: +33 5 61 55 30 03.
** Corresponding author at: Université de Toulouse, UPS, INPT, Laboratoire de Génie Chimique, 118 route de Narbonne, F-31062 Toulouse, France. Tel.: +33 5 61 55 60 73; fax: +33 5 61 55 61 39.
E-mail addresses: Katia.Fajerwerg@lcc-toulouse.fr (K. Fajerwerg), evrard@chimie.ups-tlse.fr (D. Evrard).
[1] ISE Member.

http://dx.doi.org/10.1016/j.electacta.2013.10.172

[26]. Indeed, the best results have been observed on small (around 20 nm diameter) [28] and very small (less than 10–15 nm) AuNPs [26,27], and for high Au(1 1 0)/Au(1 1 1) ratio, Au(1 0 0) faces being not present in small NPs [24]. Wain has postulated that small NPs possess high fractions of high index steps, edges and kink sites which may favor electrocatalysis [26]. In alkaline solution ORR is known to be faster than in acidic media [3]. A similar trend has been reported with respect to AuNPs structure, the activity toward O_2 reduction decreasing in the order Au(1 0 0) ≫ Au(1 1 0) > Au(1 1 1) [29]. However, the size effect is not as clear as in the case of acidic media: Tang et al. have noticed ORR kinetics to be 2.5 times higher on 3 nm diameter AuNPs supported on carbon than on 7 nm ones [30], whereas Lee et al. have observed better results on 8 nm NPs compared to 3 and 6 nm ones [31]. El-Deab et al. have also reported an interesting study in which relatively big AuNPs (ca. 50–300 nm) were selectively enriched in the most active crystallographic faces, namely Au(1 0 0) and Au(1 1 0), and exhibited better kinetic activity toward the ORR than smaller (ca. 10–40 nm) NPs [32]. AuNPs shape has also been reported to have an influence on their electrocatalytic response [33,34]. For instance, Kuai et al. have shown that icosahedral AuNPs exhibited enhanced electrocatalytic performances toward ORR and have proposed their multiple-twinned structure to be more chemically active because of their high surface-defect density [34].

Surprisingly, there are very few reports dealing with ORR on AuNPs in neutral media, although such studies would be of great interest for biological or medical topics [35,36]. Raj et al. have highlighted the electrocatalytic effect of AuNPs anchored by different organic layers on bare Au electrodes toward the ORR in phosphate buffer solution (pH 7.2) [37]. In the case of AuNPs stabilized by cystamine, the 2-electron reduction of O_2 into H_2O_2 has been found to occur at a potential 130 mV higher than on polycrystalline Au electrode. Although the resulting peak current was enhanced 1.2 times compared to an unmodified electrode, no kinetic feature has been provided in this study. Shim et al. have reported the comparison of the ORR kinetics on bulk Au and AuNPs in phosphate buffer (pH 7.4) and have shown the influence of the electrode pretreatment, i.e. 200 successive potential scans in 1 M H_2SO_4 [38]. A Koutecky–Levich mathematical treatment of the steady-state voltammetric curves has been performed but its exploitation has been limited to the determination of the number of electrons n exchanged. Only El-Deab et al. have conducted a more detailed kinetic study upon ORR in neutral phosphate buffer solution by combining Koutecky–Levich analysis with rotating Pt ring GC disk electrode measurements [39]. The values of n have been obtained at various potentials and an interesting estimation of the energy savings during H_2O_2 production has been proposed. However this latter work did not go as far as the determination of kinetic parameters such as cathodic transfer coefficients βn so that there is a lack for kinetic data upon ORR in neutral media. Very recently, we have reported a complete kinetic study of ORR in several neutral solutions on glassy carbon (GC) and bulk Au [40]. In the present work, we describe the performances of AuNPs deposited on GC by constant potential electrolysis (CPE) using various deposition durations and potentials with respect to ORR in a NaCl–$NaHCO_3$ (0.15 M/0.028 M, pH 7.4) neutral medium. The different deposits were characterized by cyclic voltammetry (CV) in H_2SO_4 and field emission gun scanning electron microscopy (FEG-SEM). Furthermore, Pb underpotential deposition (UPD) experiments were conducted in order to gain information on the structure of the AuNPs. The data obtained upon structure, size and density of the deposits were correlated to the cathodic transfer coefficients βn determined using the Koutecky–Levich method. Finally, these βn values were compared to those previously obtained in the same neutral media on bulk materials.

2. Experimental

2.1. Chemicals and apparatus

All the solutions were prepared using ultra pure water (Milli-Q Millipore, 18.2 MΩ cm). $HAuCl_4 \cdot 3H_2O$ (pro analysis grade) was purchased from Acros Organics. $NaNO_3$ (suprapur grade) and $Pb(NO_3)_2$ (analytical grade) were obtained from Merck. 95% H_2SO_4 (normapur grade) and 37% HCl were supplied by VWR Prolabo. 70% $HClO_4$ was purchased from Aldrich. NaCl and $NaHCO_3$ (analytical grade) were from Fisher Scientific.

Except the electrode activation which was performed at room temperature, all the experiments were performed at controlled temperature using a Fisher Scientific Isotemp thermoregulator.

All the electrochemical experiments were carried out in a standard three-electrode water-jacketed cell using a μ-Autolab II potentiostat (Metrohm) interfaced to a personal computer controlled with NOVA 1.9 software package (Metrohm). A Metrohm Ag/AgCl/KCl 3 M electrode, separated from the electrochemical cell by a Teflon PTFE capillary containing the support electrolyte solution and terminated by a ceramic diaphragm (D type), and a Metrohm glassy carbon (GC) wire were used as reference and counter electrodes, respectively. All the potentials given in the text and the figures are referred to SHE ($E_{Ag/AgCl/KCl\ 3\ M}$ = 0.199 V vs. SHE). Working electrodes were GC (d = 3 mm, A = 7.069 mm^2) and Au (d = 2 mm, A = 3.142 mm^2) rotating disk electrodes from Radiometer. Gold nanoparticles modified GC (AuNPs-GC) electrodes were prepared using GC plates from OrigaLys ElectroChem SAS (d = 5.5 mm, A = 23.758 mm^2). The corresponding value of geometrical surface area A was used to calculate current densities from currents. When necessary, working electrodes were rotated using a rotating system Model EDI 101 interfaced with a CTV 101 speed control unit from Radiometer.

When indicated, the solutions were deaerated using a N_2 stream for 15 min. A N_2 atmosphere was also maintained over the solution during the corresponding experiments.

2.2. Electrode preparation and modification

All the working electrodes were carefully polished prior to use. All electrodes were first polished by silicon carbide grinding paper (grit 1200) for 10 s. GC surfaces were polished successively by a 9 μm, 3 μm, 1 μm and 0.25 μm diamond suspension (Presi) on a cloth polishing pad during 2 min for each size. Au electrodes were polished by 5 μm, 1 μm and 0.3 μm alumina slurry (Presi) on a cloth polishing pad during 2 min for each size. Between each polishing step, the surfaces were cleaned with MilliQ water. Finally, all electrodes were rinsed in an ultrasonic 96% ethanol bath (three times for 10 min) and cleaned with MilliQ water. After drying, the quality of the polishing step was verified by checking the surface state using a Nikon Eclipse LV150 optical microscope.

AuNPs were electrodeposited at 10 °C onto GC plates using constant potential electrolysis (CPE) at a given potential (from −0.3 V to 0.7 V) for various times (between 10 s and 1800 s) from a deaerated 0.1 M $NaNO_3$ solution containing 0.25 mM $HAuCl_4$ (pH = 3). The resulting AuNPs-GC electrodes were then carefully rinsed using MilliQ water and activated in a deaerated 0.5 M H_2SO_4 solution by running 30 scans between 0.2 V and 1.6 V at a scan rate of 100 mV s^{-1}.

2.3. AuNPs characterization

The AuNPs-GC surface was characterized by field emission gun scanning electron microscopy (FEG-SEM) using Quanta 250 FEG FEI equipment with an accelerating voltage of 5 kV and a working distance between 3 and 8 mm depending on the sample. Image

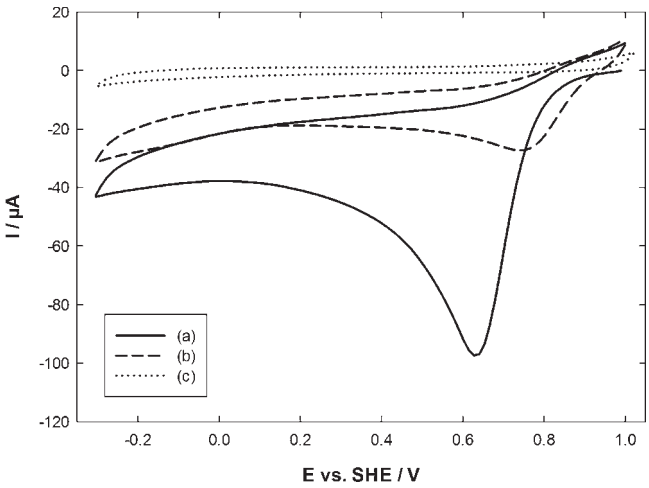

Fig. 1. CVs recorded on a GC electrode in a deaerated 0.1 M $NaNO_3$ solution containing 0.25 mM $HAuCl_4$: (a) first and (b) second scan; (c) CV recorded in the same conditions in the absence of $HAuCl_4$. Scan rate: 50 mV s^{-1}.

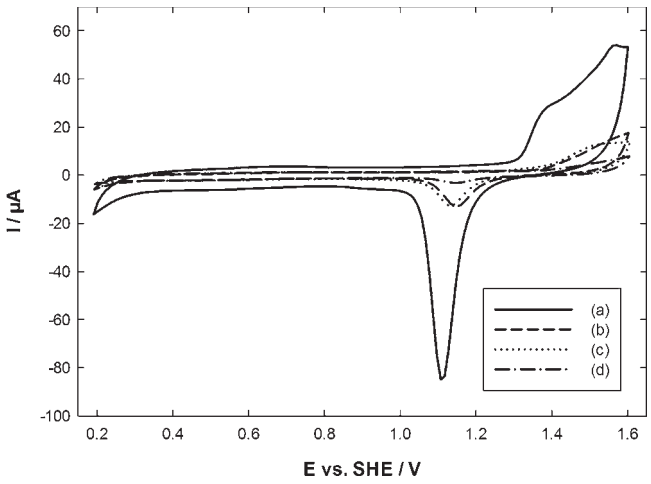

Fig. 2. Last of the 30 consecutive scans recorded by CV in a 0.5 M H_2SO_4 solution on AuNPs-GC electrodes prepared by CPE using the following conditions: (a) −0.3 V/1800 s; (b) −0.3 V/10 s; (c) 0.7 V/1800 s; (d) 0.7 V/10 s. Scan rate: 100 mV s^{-1}.

analysis was carried out using a homemade program for particles counting (density estimation) and average diameter measurement developed using MatLab image processing toolbox software. The density and average size of AuNPs were evaluated from a 85.3 μm^2 GC surface analysis counting a minimum of 40 and 4000 particles (depending on the charge used during the electrodeposition step). For each deposit, the error was calculated from the analysis of at least three different SEM images using the adequate magnification.

Pb underpotential deposition (UPD) experiments were conducted in a 0.01 M $HClO_4$ solution containing 10^{-3} M $Pb(NO_3)_2$. A potential step of −0.2 V was applied for 10 s before stripping from −0.2 V to 0.6 V at 50 mV s^{-1}.

2.4. Oxygen reduction

Electrochemical reduction of O_2 on unmodified and modified electrodes was performed at 20 °C in an aerated $NaCl/NaHCO_3$ (0.15 M/0.028 M – pH 7.4) solution by using linear sweep voltammetry and different electrode rotation rates (from 600 rpm to 2600 rpm). The electrode potential was swept from the open circuit potential (ocp) to that corresponding to hydrogen evolution at a potential scan rate of 1 mV s^{-1}.

3. Results and discussion

3.1. AuNPs electrodeposition

The cyclic voltammogram (CV) of a deaerated 0.1 M $NaNO_3$ solution containing 0.25 mM $HAuCl_4$ was recorded on GC in order to choose the parameters for AuNPs electrodeposition (Fig. 1). $NaNO_3$ was used as supporting electrolyte in order to avoid coalescence phenomena, as previously reported in the literature [41]. On the first forward scan (Fig. 1, solid line), one single reduction peak was noticed at 0.63 V which was absent when recording CV in Au(III)-free $NaNO_3$ solution (Fig. 1, dotted line). It is related to the well-known three-electron reduction process of Au(III) which leads to the formation of metallic AuNPs on the electrode surface (Eq. (4)) [42–45]:

$$AuCl_4^- + 3e^- \rightarrow Au + 4Cl^- \quad E^\circ = 1.00\,V/SHE \qquad (4)$$

On the second forward scan (dashed line), this peak was shifted 110 mV to higher potential values, in accordance with thermodynamics which predicts an easier growth of previously formed AuNPs than nucleation of new AuNPs on GC electrode [44–47]. It has to be noted that this phenomenon was not accompanied by a current crossover on the first backward scan, contrary to what has been described in many reports including our own works [42–45]. This may be explained taking into account first, the relatively low difference of energy required for the reduction of Au on GC and on Au (as shown by the little potential shift of Au(III) reduction peak between first and second forward scans, respectively) and second, the very cathodic inversion potential (−0.3 V) which induced an important contribution of the diffusion according to Cottrell's law (current proportional to $t^{-1/2}$).

In this work, AuNPs were electrosynthesized using CPE, considering our previous work showing that it is the best electrodeposition mode to get NPs with controlled size and density [45]. To get different AuNPs deposits, both electrolysis potential and duration were varied. From the analysis of Fig. 1, CPE were performed at two "extreme" potentials, i.e. −0.3 V and 0.7 V for 10 s and 1800 s.

3.2. AuNPs characterization

The four different AuNPs deposits were first activated and characterized by recording CV in 0.5 M H_2SO_4 [43,48]. Fig. 2 presents the last of the 30 consecutive scans recorded for each deposit. At this stage of the experiment, no evolution was noticed between one and following scan. Whatever the electrodeposition conditions, two phenomena were observed: first, the formation of Au "oxides" between 1.3 and 1.6 V during the forward scan and second, the reduction of these latter around 1.13 V during the backward scan. These global considerations are consistent with previously reported results [44,45,48]. The charges corresponding to AuNPs formation ($Q_{Au(III)}$), electrodeposited AuNPs oxidation ($Q_{Au(0)}$) and Au oxide-like reduction (Q_{oxides}) are summarized in Table 1. From these values, it clearly appears that the most efficient deposition is CPE at −0.3 V for 1800 s considering the amount of deposited Au ($Q_{Au(III)}$ = 9.7 mC). Moreover, for a given CPE duration, the most efficient deposition occurred at −0.3 V. In other words, the most efficient deposition mode requires the highest cathodic overpotential with the longest time. This has already been observed by several authors [43,48,49] and is consistent with literature data which reports that high overpotentials favor instantaneous nucleation [42]. Thus, CPE at −0.3 V allows the formation of more numerous nuclei than when performed at 0.7 V whatever the electrolysis duration. As a consequence, the Au active surface area is much more important when depositing at −0.3 V, as can be seen by comparing curves (*a*) and (*c*), and (*b*) and (*d*) from Fig. 2 and the

Table 1
Characteristic of AuNPs on GC and cathodic transfer coefficient βn for the ORR for each electrodeposition conditions.

Deposit no.	Electrodeposition parameters	$Q_{Au(III)}$ (mC)[a]	$Q_{Au(0)}$ (μC)[b]	Q_{oxides} (μC)[c]	Density (μm^{-2})[d]	Average diameter (nm)[d]	βn
1	0.7 V/10 s	0.07	0.7	0.2	9 ± 2	86 ± 20	0.45 ± 0.03
2	0.7 V/1800 s	2.2	1.1	0.7	0.5 ± 0.1	315 ± 89	0.29 ± 0.03
3	−0.3 V/10 s	0.2	0.7	1.0	465 ± 30	10 ± 5	0.38 ± 0.19
4	−0.3 V/1800 s	9.7	7.3	8.3	555 ± 49	25 ± 12	0.61 ± 0.03

[a] $Q_{Au(III)}$ is the charge consumed during the electroreduction step by CPE in 0.1 M $NaNO_3$ containing 0.25 mM $HAuCl_4$.
[b] $Q_{Au(0)}$ is the charge consumed in the potential range from 1.35 and 1.6 during the formation of Au oxide-like on AuNPs deposits in 0.5 M H_2SO_4.
[c] Q_{oxides} is the charge corresponding to the reduction of Au oxide-like in 0.5 M H_2SO_4.
[d] See Section 2 for details on NPs density and average diameter estimation.

corresponding Q_{oxides} values from Table 1. It is noteworthy that the amounts of charge consumed for Au oxide-like formation and their reduction exhibited comparable values for each deposit except the one performed at 0.7 V for 10 s. In this latter case, the Q_{oxides} value was found to be 3.5 times lower than the corresponding $Q_{Au(0)}$, thus suggesting an instability of these nuclei. It may be assumed that these nuclei rearrange while oxidized or even dissolve before their reduction takes place during the backward scan.

All these results were confirmed by FEG-SEM analyses (Fig. 3). The four micrographs showed that CPE at −0.3 V afforded much more dense deposits of smaller AuNPs than CPE at 0.7 V (see Table 1 for quantitative features upon size and density). In the former case, the AuNPs were relatively small and almost hemispherical-shaped, and homogeneously distributed on the GC surface. Whatever the electrolysis time at −0.3 V, the deposits were very dense, in accordance with the fact that high cathodic overpotentials favor nucleation processes [42]. The AuNPs density for both deposits was in the same order of magnitude (465 and 555 μm^{-2} for 10 and 1800 s, respectively). It has to be noticed that the little difference in density between the 10 s and 1800 s deposits may not be due to longer reduction duration but to the impossibility for the counting software to detect very small nuclei. Anyway, increasing the electrodeposition time led to slightly bigger AuNPs and still homogeneous deposits. This is consistent with our work [45] and Finot et al.'s one [49] who showed the influence of the overpotential on nucleation/growth processes. In the former work, low cathodic overpotential associated to long electrolysis duration led to "popcorn-like" aggregates, whereas in the latter one high cathodic overpotential afforded more homogeneous deposits than low one [49]. On the contrary, performing electrodeposition at 0.7 V led to very sparse deposits of big AuNPs, even for low electrolysis time. Increasing the electrolysis duration induced a significant increase in particles diameter, leading to the formation of very big, raspberry-like AuNPs (Fig. 3b, inset).

In order to get more information upon AuNPs structuration, Pb underpotential deposition (UPD) experiments were performed in $HClO_4$ [50–52]. This technique consists in the deposition of a monolayer or submonolayer of Pb on another metal at a potential more positive than that of bulk Pb deposition. It is structure sensitive and allows crystallographic faces information to be obtained [53]. In our case, a deposition potential of −0.2 V was chosen. This technique has been recently used by several authors to identify the crystallographic faces of AuNPs. The stripping peaks can be assigned by comparison with the literature data for single crystals and polycrystalline gold [33,54–56]. The stripping steps for each AuNPs deposit are summarized in Fig. 4. The very weak response obtained for the AuNPs deposited by CPE at 0.7 V for 10 s is consistent with the $Q_{Au(III)}$ value corresponding to electrodeposition (Table 1) and did

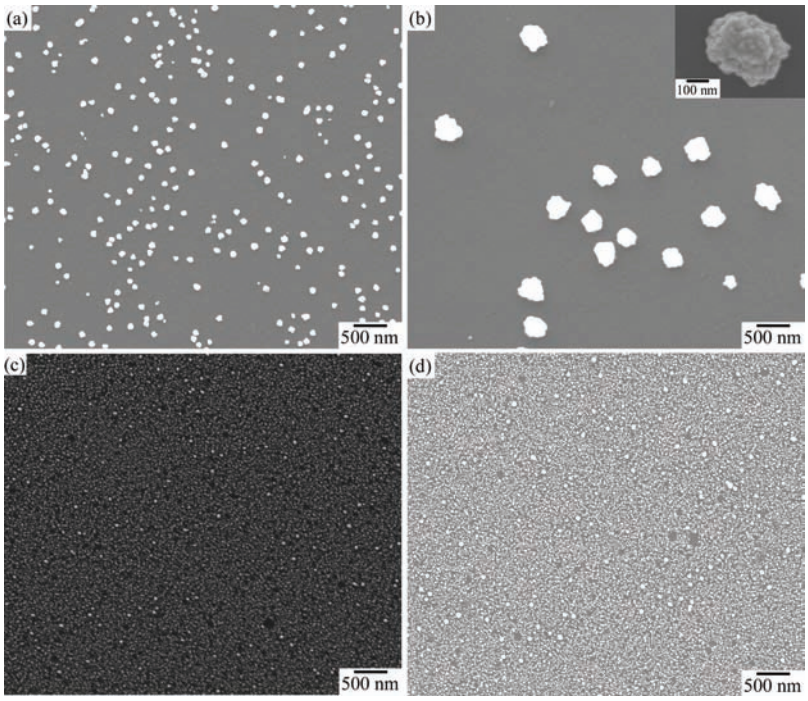

Fig. 3. FEG-SEM images of AuNPs-GC electrodes prepared from a deaerated 0.1 M $NaNO_3$ solution containing 0.25 mM $HAuCl_4$ by CPE at 0.7 V for (a) 10 s and (b) 1800 s and at −0.3 V for (c) 10 s and (d) 1800 s.

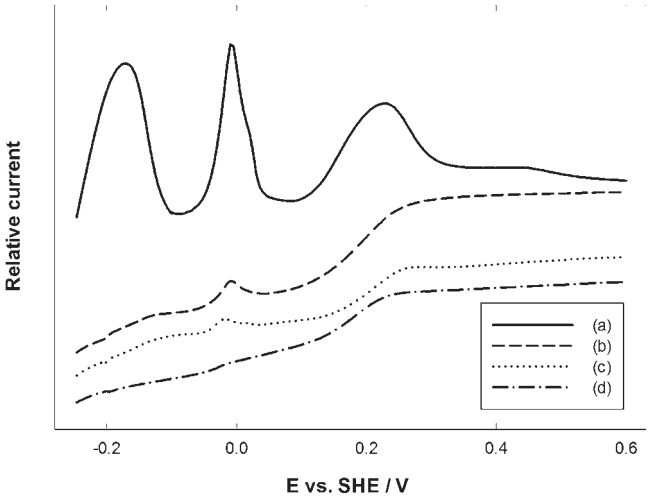

Fig. 4. Stripping step of Pb underpotential deposition recorded in a 0.01 M $HClO_4$ solution containing 10^{-3} M $Pb(NO_3)_2$ on AuNPs-GC electrodes prepared by CPE at −0.3 V for (a) 1800 s and (b) 10 s and at 0.7 V for (c) 1800 s and (d) 10 s. Pb deposition conditions: −0.2 V for 10 s; scan rate: 50 mV s^{-1}.

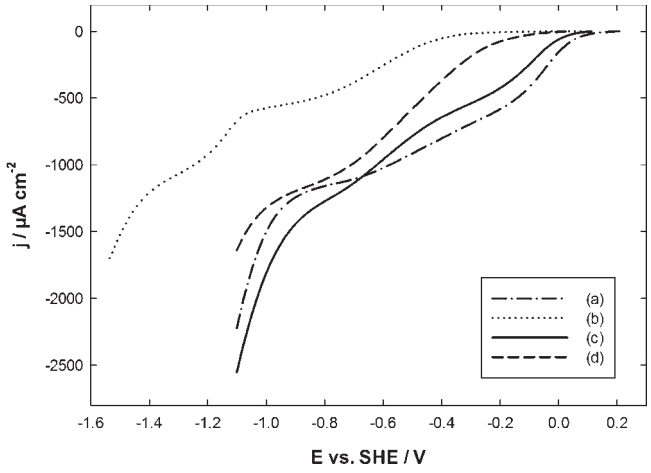

Fig. 5. Steady-state voltammograms recorded in an aerated NaCl–$NaHCO_3$ (0.15 M/0.028 M, pH 7.4) solution on: (a) bulk Au; (b) unmodified GC; AuNPs-GC electrodes prepared by CPE for 1800 s at: (c) −0.3 V; (d) 0.7 V. Scan rate: 1 mV s^{-1}.

not allow any information to be extracted. The AuNPs deposited at −0.3 V for the same time exhibited a well-defined peak at 0 V typical of (1 1 1)-oriented terraces [51,52]. Although the global electrochemical response is little, the observation of this peak is in accordance with the large amount deposition of Pb on Au(1 1 1) faces reported by several authors [50,56]. The AuNPs deposited at 0.7 V for 1800 s exhibited the same peak at 0 V associated to a small shoulder at 0.02 V. These latter were poorly defined due to the low size of the surface domains [55]. However the split of the peak at 0 V is indicative of different size domains, the peak itself being associated to wide Au(1 1 1) faces whereas the shoulder is rather related to narrower Au(1 1 1) domains [55]. Due to a much greater amount of deposited Au (see the $Q_{Au(III)}$ values in Table 1), the AuNPs deposited at −0.3 V for 1800 s exhibited a well-defined electrochemical response, the global shape of which being consistent with a polyoriented Au deposit [57]. A clear, split peak at 0 V was noticed for the Au(1 1 1) faces together with two broad signals centered at −0.15 V and 0.23 V, respectively. By comparison with literature data, this signal may be attributed to Au(1 1 0) faces [54,55]. The broad signal around −0.15 V has been observed several times for polyoriented Au [33,54,57] but has never been clearly attributed. Interestingly, no characteristic signal of Au(1 0 0) faces around 0.05 V [52] was observed on the voltammograms, whatever the deposit considered. Finally, it was verified that unmodified GC surfaces did not undergo any electrochemical response toward Pb UPD (not shown).

3.3. Kinetics study of ORR on AuNPs-GC electrodes

Fig. 5 compares the steady-state voltammograms recorded in an aerated NaCl–$NaHCO_3$ (0.15 M/0.028 M – pH 7.4) solution on bulk Au, unmodified GC, and AuNPs-GC electrodes prepared by CPE at −0.3 V and 0.7 V for 1800 s. For the sake of clarity, the voltammograms obtained using AuNPs deposits with shorter electrolysis duration were not provided. It has to be noticed that these latter deposits exhibited poor repeatability. In the neutral medium used the two consecutive two-electron reduction steps of O_2 occurred at very close half-wave potentials on bulk Au (Fig. 5a), ca. −0.1 V and −0.4 V for O_2 and H_2O_2 reduction, respectively. In particular, the second wave associated to H_2O_2 evolution was relatively ill-defined, starting from −0.2 V. On the contrary, on unmodified GC electrode O_2 and H_2O_2 reduction reactions were noticed at distinct potentials, ca. −0.6 V and −1.2 V, respectively (Fig. 5b). The large cathodic shift observed clearly illustrated the slower heterogeneous electronic transfer kinetics of ORR on GC. These results have been extensively discussed in our recent work [40]. AuNPs-GC electrodes exhibited significantly enhanced kinetics for the ORR compared to unmodified GC (Fig. 5c and d), in accordance with the results previously reported by El-Deab et al. [39]. It is noteworthy that the kinetics properties of the functionalized electrodes were found to be strongly dependent on the AuNPs size and density. The AuNPs-GC electrode prepared by CPE at 0.7 V exhibited one single 4-electron wave for O_2 reduction centered at −0.55 V (Fig. 5d) whereas on the AuNPs-GC electrode prepared by CPE at −0.3 V two bielectronic waves at −0.1 V and −0.6 V were noticed, respectively (Fig. 5c). This latter electrode afforded faster kinetics than the former one and properties very close to bulk Au (Fig. 5a). This is consistent with the observation that decreasing AuNPs size induces a decrease in cathodic overpotential [27,38] and a better selectivity for the two consecutive bielectronic oxygen reduction waves. Indeed, compared to bulk material, the two waves of ORR appeared in our case slightly better separated.

To go into further detail steady-state voltammograms were recorded on both AuNPs-GC electrodes prepared by CPE at −0.3 V and 0.7 V for 1800 s at various electrode rotation rates ω (Fig. 6A and B respectively). From the ocp potential to around the early stage of the O_2 reduction wave the current was found to be independent on ω whatever the electrode considered, indicating a charge transfer limited reaction rate. For lower potentials the cathodic current increased while increasing ω in accordance with the Levich equation (proportional to $\omega^{1/2}$). For both electrodes (Fig. 6A and B) the current plateau of the O_2 reduction wave corresponding to mass transfer limitation was poorly defined as an evidence for a mixed kinetic-diffusion control mechanism for the ORR. All these observations compare favorably with our previous results obtained on bulk Au [40]. The ill-define plateau may also be due to a variation of the number of electrons n consumed by the reduction reaction while decreasing the potential, as suggested by several authors [28,58]. The data obtained from Fig. 6A and B were analyzed using the Koutecky–Levich relation [59]:

$$\frac{1}{j} = \frac{1}{j_k} + \frac{1}{j_d} = -\frac{1}{nFkC} - \frac{1}{0.62nFD^{2/3}\omega^{1/2}\upsilon^{-1/6}C}$$

where j_k and j_d are the kinetic limited and mass transfer controlled current densities, respectively, F is the Faraday constant (96,500 C mol^{-1}), k is the potential-dependent charge transfer rate constant, C is the dioxygen bulk concentration (0.24×10^{-6} mol cm^{-3} under atmospheric pressure) [60], D is the

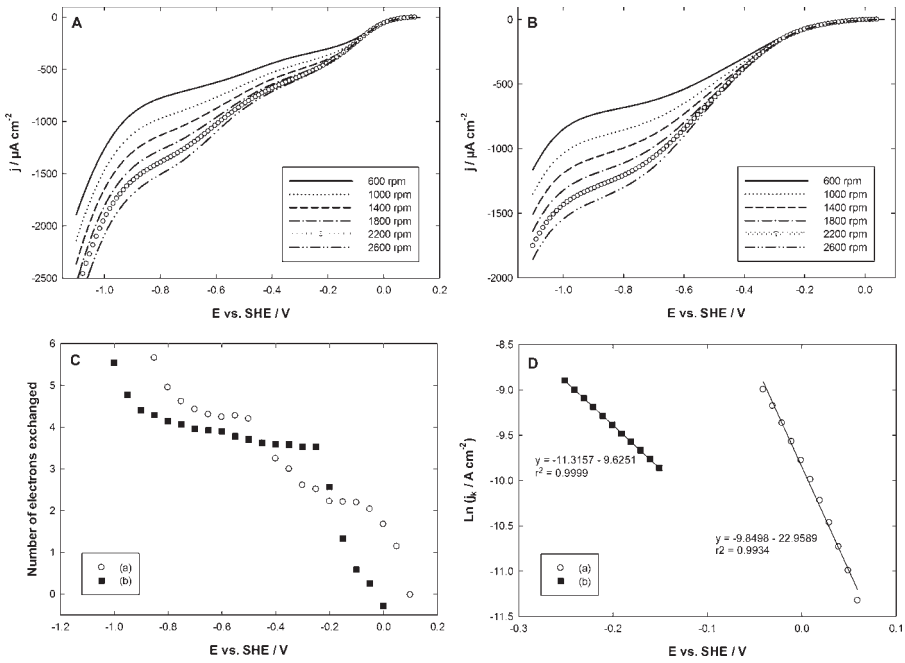

Fig. 6. (A) Steady-state voltammograms recorded in an aerated NaCl–$NaHCO_3$ (0.15 M/0.028 M, pH 7.4) solution using different electrode rotation rates ω on AuNPs-GC electrodes prepared by CPE for 1800 s at −0.3 V. Scan rate: 1 mV s^{-1}. (B) Steady-state voltammograms recorded in an aerated NaCl–$NaHCO_3$ (0.15 M/0.028 M, pH 7.4) solution using different electrode rotation rates ω on AuNPs-GC electrodes prepared by CPE for 1800 s at 0.7 V. Scan rate: 1 mV s^{-1}. (C) Variation of the number of electrons exchanged during the ORR as a function of the electrode potential. Values extracted from the Koutecky–Levich treatment applied to the steady-state voltammograms recorded in an aerated NaCl–$NaHCO_3$ (0.15 M/0.028 M, pH 7.4) solution (Fig. 5) on AuNPs-GC electrodes prepared by CPE for 1800 s at: (a) −0.3 V; (b) 0.7 V. (D) Variation of the kinetic-limited current density $\mathrm{Ln}\, j_k$ of the ORR as a function of the potential applied to the electrode. Values deduced from the steady-state voltammograms recorded in an aerated NaCl–$NaHCO_3$ (0.15 M/0.028 M, pH 7.4) solution on AuNPs-GC electrodes prepared by CPE for 1800 s at: (a) −0.3 V; (b) 0.7 V.

diffusion coefficient (1.96×10^{-5} cm^2 s^{-1}) [61,62], and ν is the kinematic viscosity of the aqueous solution (0.01 cm^2 s^{-1}) [63]. According to this latter equation the inverse of the current density j^{-1} was plotted as a function of $\omega^{-1/2}$ for different potentials in the range from 0.05 V to −1 V (not shown). All these curves exhibited a linear trend, the slope of which allowed the total number of electrons to be determined for each potential (Fig. 6C). The two AuNPs-GC electrodes clearly presented different behavior toward the ORR. For the deposit prepared by CPE at −0.3 V, the number of electrons consumed reached 2 as early as −0.05 V, indicating that the H_2O_2 production step was limited by mass transfer from this potential (Fig. 6A). From −0.2 V the number of electrons increased up to 4 at potential around −0.5 V as a consequence of the completion of the reduction process leading to the formation of H_2O. The values of the number of electrons slightly higher than 4 which were observed from −0.5 V to −0.65 V may be assumed to result from water reduction which starts in this potential range. On the contrary, using the deposit prepared by CPE at 0.7 V, the ORR started at more cathodic potential (ca. −0.05 V) and the number of electrons directly increased up to 4 for potential around −0.25 V, confirming that no intermediary two-electron step occurred on this electrode (Fig. 6B).

From the intercepts of the Koutecky–Levich plots the kinetic limited current densities contribution j_k were obtained for both AuNPs-GC electrodes. The corresponding plots of $\mathrm{Ln}\, j_k$ as a function of the potential (Fig. 6D) allowed the cathodic transfer coefficient βn to be calculated from the charge transfer rate constant k:

$$k = k^{\circ} \exp\left(-\frac{\beta n F}{RT}(E - E^{\circ\prime})\right)$$

where k° (cm s^{-1}) is the intrinsic charge transfer rate constant, R is the gas constant (8.31 J mol^{-1} K^{-1}), and $E^{\circ\prime}$ is the apparent standard potential. The values found for the βn were 0.61 and 0.29 for the AuNPs deposits prepared by CPE at −0.3 V and 0.7 V respectively. Considering the number of electrons exchanged in each case (as shown in Fig. 6C) the effective β values are 0.30 and 0.07. This makes evidence for the better kinetics results obtained for the ORR using the most cathodic deposits. The βn values calculated for the short electrolysis duration deposits are also presented in Table 1, although the poor repeatability of the voltammograms made them hard to obtain. This lack of repeatability may be attributed to rearrangements of the AuNPs during the voltammetric measurements due to potentiodynamic perturbation, or even to dissolution of the smallest AuNPs [45,64,65]. The comparison of all four deposits reinforces the correlation between low-size AuNPs obtained by very low deposition potentials and better kinetics results (see βn values in Table 1). The values obtained for the βn also compare favorably with those we reported in the same neutral medium on bulk Au and unmodified GC electrodes, ca. 0.39 and 0.24 respectively [40].

Finally a more complete set of AuNPs deposits was prepared by varying the potential applied for CPE every 0.25 V from −0.3 V to 0.7 V and using electrolysis duration of 10, 60, 300, 600 and 1800 s. For each experimental condition the corresponding βn value was calculated as previously described. Fig. 7 depicts a graphical representation of these values as a function of both electrolysis potential and duration. From this representation, a well-defined area was noticed which corresponds to the higher βn values. This area is clearly positioned in the part of the graph corresponding to the lowest electrolysis potentials and the longest electrolysis times, confirming the trend observed with the first two deposits. Thus, from the kinetic point of view the best results were obtained for electrodes which exhibited dense deposits of relatively small AuNPs. This is in accordance with our previous works in which we assumed that in such a case the deposit may be viewed as an array of spherical-shaped Au “nanoelectrodes” which act together

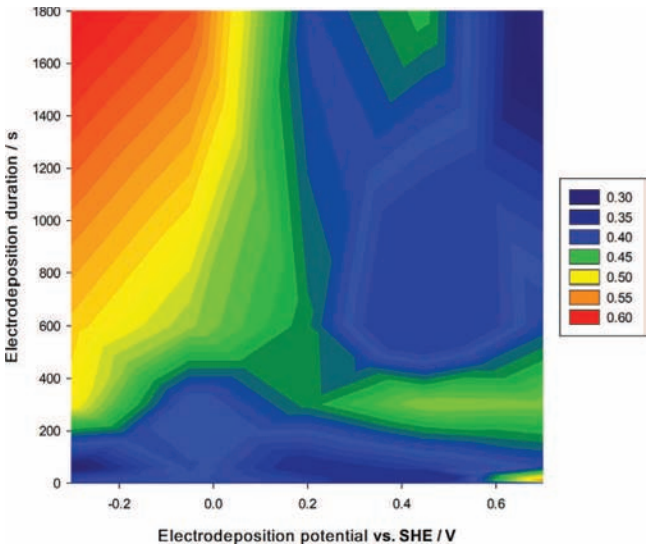

Fig. 7. Evolution of the cathodic transfer coefficient βn corresponding to the ORR in an aerated NaCl–$NaHCO_3$ (0.15 M/0.028 M, pH 7.4) solution on AuNPs-GC electrodes as a function of the potential (x axis) and duration (y axis) used to prepare the deposits by CPE.

[44,45]. This is also consistent with Wain's work who showed that the best results with respect to ORR were obtained on the smallest AuNPs, which exhibited the highest Au(1 1 0)/Au(1 1 1) ratio [26]. In our case, the presence of very small AuNPs or even nanoclusters [66] which would strongly contribute to the global response of the modified electrodes cannot be excluded [67], although the magnification of the SEG-FEM micrographs was not high enough to allow their observation.

4. Conclusions

In this work, AuNPs were electrodeposited onto GC electrodes by constant potential electrolysis. Both AuNPs size and density were found to be strongly dependent on the electrolysis parameters, the smallest NPs (25 nm) with highest density (555 μm^{-2}) being obtained with the highest cathodic overpotential ($E = -0.3$ V) and the longest electrolysis time (1800 s). The response of the deposits toward the ORR was examined in a NaCl–$NaHCO_3$ (0.15 M/0.028 M, pH 7.4) neutral medium. From the Koutecky–Levich treatment of the current–potential curves, the value of the number of electrons n exchanged during the reaction was extracted. The results revealed a direct 4-electron reduction pathway for O_2 on AuNPs electrogenerated by CPE at 0.7 V, whereas two successive bielectronic steps were evidenced on AuNPs obtained using higher cathodic overpotential. In this last case the AuNPs-GC electrodes exhibited significantly enhanced kinetics for ORR with much higher βn values (0.61) compared to bulk Au (0.39) and unmodified GC (0.24). These values were found to be strongly correlated to the physico-chemical characteristics of the AuNPs deposits. The best results are obtained using the deposits exhibiting the smallest NPs and the highest density. On the basis of these data, works are in progress which aim at developing new nanoparticle-based sensors for O_2 determination in neutral media.

Acknowledgements

The authors thank the Pôle de Recherche et de l'Enseignement Supérieur (PRES) Toulouse and the Région Midi-Pyrénées for financial support and Yannick Hallez for his help in MATLAB programming.

References

[1] M.T.M. Koper, H.A. Heering, Comparison of electrocatalysis and bioelectrocatalysis of hydrogen and oxygen redox reactions *in* Fuel cell science, in: A. Wieckowski, J.K. Norskov (Eds.), Theory, fundamentals and biocatalysis, John Wiley & Sons, Hoboken, 2010, p. 71.
[2] J.A. Keith, T. Jacob, Computational simulations on the oxygen reduction reaction in electrochemical systems, Mod. Aspect Electrochem. 50 (2010) 89.
[3] P. Quaino, N.B. Luque, R. Nazmutdinov, E. Santos, W. Schmickler, Why is gold such a good catalyst for oxygen reduction in alkaline media? Angew. Chem. Int. Ed. Engl. 51 (2012) 12997.
[4] A. Radoslav, Recent Advances in the Kinetics of Oxygen Reduction, Wiley VCH, New York, 1998.
[5] J. Jacq, O. Bloch, Réduction électrochimique de l'oxygène en eau oxygénée. Etablissement de l'équation de la courbe de polarisation: application au calcul des paramètres thermodynamiques et cinétiques des étapes élémentaires, Electrochim. Acta 15 15 (1970) 1945.
[6] R.W. Zurilla, R.K. Sen, E. Yeager, The kinetics of the oxygen reduction reaction on gold in alkaline solution, J. Electrochem. Soc. 125 (1978) 1103.
[7] A.J. Appleby, Electrocatalysis of aqueous dioxygen reduction, J. Electroanal. Chem. 357 (1993) 117.
[8] I. Kazeman, M. Hasanzadeh, M. Jafarian, N. Shadjou, B. Khalilzadeh, Oxygen reduction reaction on a rotating Ag-GC disk electrode in acidic solution, Chin. J. Chem. 28 (2010) 504.
[9] A. Damjanovic, V. Brusic, J.O.M. Bockris, Mechanism of oxygen reduction related to electronic structure of gold-palladium alloy, J. Phys. Chem. 71 (1967) 2741.
[10] D.T. Sawyer, G. Chiericato, T. Tsuchiya Jr., C.T. Angelis, E.J. Nanni Jr., Effects of media and electrode materials on the electrochemical reduction of dioxygen, Anal. Chem. 54 (1982) 1720.
[11] E. Yeager, Electrocatalysts for molecular oxygen reduction, Electrochim. Acta 29 (1984) 1527.
[12] E. Yeager, Dioxygen electrocatalysis. Mechanisms in relation to catalyst structure, J. Mol. Catal. 38 (1986) 5.
[13] D.S. Gnanamuthu, J.V. Petrocelli, A generalized expression for the Tafel slope and the kinetics of oxygen reduction on noble metals and alloys, J. Electrochem. Soc. 114 (1967) 1036.
[14] J.W. Severinghaus, P.B. Astrup, History of Blood Gas Analysis, Little, Brown, and Co. Inc., San Francisco, 1987.
[15] J.W. Severinghaus, History of measuring O_2 and CO_2 responses, Adv. Exp. Med. Biol. 605 (2008) 3.
[16] G. Strukul, Catalytic Oxidations with Hydrogen Peroxide as Oxidant, Springer, Dordrecht, 1992.
[17] D. Brondel, R. Edwards, A. Hayman, D. Hill, S. Mehta, T. Semerad, Corrosion in the oil industry, Oilfield Rev. 6 (1994) 4.
[18] A.J. Appleby, F.R. Foulkes, Fuel Cell Handbook, Van Nostrand Reinhold, New York, 1989.
[19] B. Wang, Recent development of non-platinum catalysts for oxygen reduction reaction, J. Power Sources 152 (2005) 1.
[20] L. Lessing, T.G. Watson, Application of oxygen to highly aerobic fermentations, South Afr. Food Rev. 9 (1982) S107.
[21] A.A. Gewirth, M.S. Thorum, Electroreduction of dioxygen for fuel-cell applications: Materials and challenges, Inorg. Chem. 49 (2010) 3557.
[22] N. Alonso-Vante, Tailoring of metal cluster-like materials for the molecular oxygen reduction reaction, Pure Appl. Chem. 80 (2008) 2103.
[23] V. Mazumder, Y. Lee, S. Sun, Recent development of active nanoparticle catalysts for fuel cell reactions, Adv. Funct. Mater. 20 (2010) 1224.
[24] G. Vázquez-Huerta, G. Ramos-Sánchez, R. Antaño-López, O. Solorza-Feria, Electrocatalysis of oxygen reduction on Au nanoparticles, ECS Trans. 20 (2009) 259.
[25] J.S. Jirkovsky, M. Halasa, D.J. Schiffrin, Kinetics of electrocatalytic reduction of oxygen and hydrogen peroxide on dispersed gold nanoparticles, Phys. Chem. Chem. Phys. 12 (2010) 8042.
[26] A.J. Wain, Imaging size effects on the electrocatalytic activity of gold nanoparticles using scanning electrochemical microscopy, Electrochim. Acta 92 (2013) 383.
[27] T. Inasaki, S. Kobayashi, Particle size effects of gold on the kinetics of the oxygen reduction at chemically prepared Au/C catalysts, Electrochim. Acta 54 (2009) 4893.
[28] M.S. El-Deab, T. Ohsaka, Hydrodynamic voltammetric studies of the oxygen reduction at gold nanoparticles-electrodeposited gold electrodes, Electrochim. Acta 47 (2002) 4255.
[29] T.J. Schmidt, V. Stamenkovic, M. Arenz, N.M. Markovic, P.N. Ross Jr., Oxygen electrocatalysis in alkaline electrolyte: Pt(hkl), Au(hkl) and the effect of Pd-modification, Electrochim. Acta 47 (2002).
[30] W. Tang, H. Lin, A. Kleiman-Shwarsctein, G.D. Stucky, E.W. McFarland, Size-dependent activity of gold nanoparticles for oxygen electroreduction in alkaline electrolyte, J. Phys. Chem. C 112 (2008) 10515.
[31] Y. Lee, A. Loew, S. Sun, Surface- and structure-dependent catalytic activity of Au nanoparticles for oxygen reduction reaction, Chem. Mater. 22 (2010) 755.
[32] M.S. El-Deab, T. Sotomura, T. Ohsaka, Ohsaka, Size and crystallographic orientation controls of gold nanoparticles electrodeposited on GC electrodes, J. Electrochem. Soc. 152 (2005) C1.
[33] J. Hernández, J. Solla-Gullón, E. Herrero, J.M. Feliu, A. Aldaz, In situ surface characterization and oxygen reduction reaction on shape-controlled gold nanoparticles, J. Nanosci. Nanotechnol. 9 (2009) 2256.

[34] L. Kuai, B. Geng, S. Wang, Y. Zhao, Y. Luo, H. Jiang, Silver and gold icosahedra. One-pot water-based synthesis and their superior performance in the electrocatalysis for oxygen reduction reaction in alkaline media, Chem. Eur. J. 17 (2011) 3482.
[35] F. King, M.J. Quinn, C.D. Litke, Oxygen reduction on copper in neutral NaCl solution, J. Electroanal. Chem. 385 (1995) 45.
[36] C.E.W. Hahn, Electrochemical analysis of clinical blood-gases, gases and vapors, Analyst 123 (1998) 57R.
[37] C.R. Raj, A.I. Abdelrahman, T. Ohsaka, Gold nanoparticle-assisted electroreduction of oxygen, Electrochem. Commun. 7 (2005) 888.
[38] J.H. Shim, J. Kim, C. Lee, Y. Lee, Electrocatalytic activity of gold and gold nanoparticles improved by electrochemical pretreatment, J. Phys. Chem. C 115 (2011) 305.
[39] M.S. El-Deab, T. Okajima, T. Ohsaka, Electrochemical reduction of oxygen on gold nanoparticle-electrodeposited glassy carbon electrodes, J. Electrochem. Soc. 150 (2003) A851.
[40] G. Gotti, K. Fajerwerg, D. Evrard, P. Gros, Gros, Kinetics of dioxygen reduction on gold and glassy carbon electrodes in neutral media, Int. J. Electrochem. Sci. 8 (2013) 12643.
[41] Y. Wang, J. Deng, J. Di, Y. Tu, Electrodeposition of large size gold nanoparticles on indium tin oxide glass and application as refractive index sensor, Electrochem. Commun. 11 (2009) 1034.
[42] L. Komsiyska, G. Staikov, Electrocrystallization of Au nanoparticles on glassy carbon from $HClO_4$ solution containing $[AuCl_4]$, Electrochim. Acta 54 (2008) 168.
[43] A.P. O'Mullane, S.J. Ippolito, Y.M. Sabri, V. Bansal, S.K. Bhargava, Premonolayer oxidation of nanostructured gold: An important factor influencing electrocatalytic activity, Langmuir 25 (2009) 3845.
[44] T. Hezard, K. Fajerwerg, D. Evrard, V. Collière, P. Behra, P. Gros, Gold nanoparticles electrodeposited on glassy carbon using cyclic voltammetry: Application to Hg(II) trace determination, J. Electroanal. Chem. 664 (2012) 46.
[45] T. Hezard, K. Fajerwerg, D. Evrard, V. Collière, P. Behra, P. Gros, Influence of the gold nanoparticles electrodeposition method on Hg(II) trace electrochemical detection, Electrochim. Acta 73 (2012) 15.
[46] G. Gunawardena, G. Hills, I. Montenegro, B. Scharifker, Electrochemical nucleation Part I. General considerations, J. Electroanal. Chem. 138 (1982) 225.
[47] D. Grujicic, B. Pesic, Electrodeposition of copper: the nucleation mechanisms, Electrochim. Acta 47 (2002) 2901.
[48] M.S. El-Deab, On the preferential crystallographic orientation of Au nanoparticles: Effect of electrodeposition time, Electrochim. Acta 54 (2009) 3720.
[49] M.O. Finot, G.D. Braybrook, M.T. McDermott, Characterization of electrochemically deposited gold nanocrystals on glassy carbon electrodes, J. Electroanal. Chem. 466 (1999) 234.
[50] A. Hamelin, Lead adsorption on gold single crystal stepped surfaces, J. Electroanal. Chem. 101 (1979) 285.
[51] A. Hamelin, Underpotential deposition of lead on single nanocrystal faces of gold, J. Electroanal. Chem. 165 (1984) 167.
[52] A. Hamelin, J. Lipkowski, Underpotential deposition of lead on gold single crystal faces. Part II General discussion, J. Electroanal. Chem. 171 (1984) 317.
[53] E. Herrero, L.J. Buller, H.D. Abruña, Underpotential deposition at single crystal surfaces of Au, Pt, Ag and other materials, Chem. Rev. 101 (2001) 1897.
[54] J. Hernández, J. Solla-Gullón, E. Herrero, A. Aldaz, J.M. Feliu, Characterization of the surface structure of gold nanoparticles and nanorods using structure sensitive reactions, J. Phys. Chem. B 109 (2005) 12651.
[55] C.M. Sánchez-Sánchez, F.J. Vidal-Iglesias, J. Solla-Gullón, V. Montiel, A. Aldaz, J.M. Feliu, E. Herrero, Scanning electrochemical microscopy for studying electrocatalysis on shape-controlled gold nanoparticles and nanorods, Electrochim. Acta 55 (2010) 8252.
[56] S. Hebié, L. Cornu, T.W. Napporn, J. Rousseau, B.K. Kokoh, Insight on the surface structure effect of free gold nanorods on glucose electrooxidation, J. Phys. Chem. C 117 (2013) 9872.
[57] C. Mitchell, M. Fayette, N. Dimitrov, Homo- and hetero-epitaxial deposition of Au by surface limited redox replacement of Pb underpotentially deposited layer in one-cell configuration, Electrochim. Acta 85 (2012) 450.
[58] G. Vázquez-Huerta, G. Ramos-Sánchez, A. Rodríguez-Castellanos, D. Meza-Calderón, R. Antaño-López, O. Solorza-Feria, Electrochemical analysis of the kinetics and mechanism of the oxygen reduction reaction on Au nanoparticles, J. Electroanal. Chem. 645 (2010) 35.
[59] J. Koutecky, The polarographic current due to an electrode process preceded by a chemical reaction in solution between reactants differing in their diffusion coefficients, Chem. Listy Vedu Prum. 47 (1953) 1758.
[60] B.B. Benson, D.J. Krause, The concentration and isotopic fractionation of oxygen dissolved in freshwater and seawater in equilibrium with the atmosphere, Limnol. Oceanogr. 29 (1984) 620.
[61] A.J. van Stroe, L.J.J. Janssen, Determination of the diffusion coefficient of oxygen in sodium chloride solutions with a transient pulse technique, Anal. Chim. Acta 279 (1993) 213.
[62] M. Jamnongwong, K. Loubiere, N. Dietrich, G. Hebrard, Experimental study of oxygen diffusion coefficients in clean water containing salt, glucose or surfactant: Consequences on the liquid-side mass transfer coefficients, J. Chem. Eng. (Amsterdam, Netherlands) 165 (2010) 758.
[63] F.J. Millero, F. Huang, A.L. Laferiere, Solubility of oxygen in the major sea salts as a function of concentration and temperature, Mar. Chem. 78 (2002) 217.
[64] G. Sandmann, H. Dietz, W. Plieth, Preparation of silver nanoparticles on ITO surfaces by a double-pulse method, J. Electroanal. Chem. 491 (2000) 78.
[65] M. Ueda, H. Dietz, A. Anders, H. Kneppe, A. Meixner, W. Plieth, Double-pulse technique as an electrochemical tool for controlling the preparation of metallic nanoparticles, Electrochim. Acta 48 (2002) 377.
[66] R. Jin, Y. Zhu, H. Qian, Quantum-sized gold nanoclusters: Bridging the gap between organometallics and nanocrystals, Chem. Eur. J. 17 (2011) 6584.
[67] W. Chen, S. Chen, Oxygen electroreduction catalyzed by gold nanoclusters: strong core size effects, Angew. Chem. Int. Ed. Engl. 48 (2009) 4386.